System-level exergetic optimization for lowering the carbon footprint of offshore production assets

Nathan.SENECHAU[ab], Maxime HIGELIN[b], Laurent AVAULLEE[b], Sabine SOCHARD[a], Sylvain SERRA[a], Jean-Michel RENEAUME[a]

[a] *Universite de Pau et des Pays de l'Adour, LaTEP, Pau, France, nathan.senechau@univ-pau.fr*
[b] *TotalEnergies SE, Pau, France*

Abstract :
The aim of this study is, on the one hand, to present the integrated exergetic modeling of a real offshore oil and gas production site off the coast of Angola called "Girassol", and on the other hand, the various dynamic optimization techniques applied to this model to compare the minimization of GHG emissions with the minimization of site irreversibilities. Firstly, the study briefly outlines the integrated model and its validation with sufficient accuracy (relative error < 1e-1). Secondly the study is focused on the gas turbine load allocation optimization problem. These optimization results enable us to confirm that the optimal solution is to distribute the power equally between the gas turbines for minimizing both GHG emissions and irreversibilities. Finally, a dynamic optimization method combining a global Bayesian exploration solver and a deterministic SQP-type solver is introduced to address the gas-lift allocation optimization problem. An average of 3 % of CO2 emissions can be saved under the historical oil production constraint. The results are presented as a Pareto front, enabling comparison between best solutions for the energy efficiency of the site and best solutions for its carbon footprint.

Keywords:
Exergy; Irreversibilities; GHG emissions; Optimization; Offshore; Oil and gas.

1. Introduction

1.2. Context

The major oil company TotalEnergies [1] has set a target to reduce its emissions by 40% compared to 2015 levels for its operated assets within scope 1 and 2 by 2030, aiming to achieve net zero by 2050. As of now, emissions have decreased by 36% in 2024, reaching 36 $MtCO_2eq$, with a carbon intensity per barrel of 17 kg CO_2eq, down from 21 $kgCO_2eq$. Between 2023 and 2025, the Company estimates [1] that about 2 $MtCO_2eq$ have been avoided through investments in electrification, improvements in energy efficiency, and the recovery of waste heat. Regarding upstream operations, particularly offshore site emissions, the Company estimates [1] that around 63% of greenhouse gas emissions from these facilities are due to the use of gas turbines, which produce approximately 65 to 75 MW of electric power to supply mechanical work to all surface equipment present on the FPSO (Floating Production Storage and Offloading). The model and digital optimization framework presented in this study focus on a real-world case of the Girassol field off the coast of Angola. Production in this field began in 2001 and is still ongoing today.

1.3. Objectives

Over the past ten years, TotalEnergies has implemented emission reporting, as well as monitoring and controlling the energy performance of its various offshore production facilities. However, the large scale, complexity, and diversity of these installations have made sensitivity analysis for operational and design improvements both time-consuming and difficult to interpret. Numerous studies [2-3] and exergy analyses [4-[9] on offshore sites have highlighted more effective energy performance indicators and identified critical subsystems responsible for the majority of irreversibilities. Nevertheless, exergy modeling and optimization of energy performance and GHG emissions have generally been limited to either the subsurface [10] or surface process scopes. However, offshore production sites such as Girassol operate through interconnected material and energy flows between surface processes and subsurface production wells at the reservoir level.

Specifically, on Girassol, production is enhanced using reinjected surface gas, a process known as “gas-lift injection.” Until now, existing models have not accounted for the feedback effect of gas lift on offshore fields. These interactions have either been considered from the surface perspective as a volume constraint for reinjection, or from the subsurface perspective as one among several activation options over time. Therefore, to optimize GHG emissions and energy performance relative to site production, it is necessary to model the entire oil field chain in an integrated manner. This requires developing a coupled subsurface-surface model that enables dynamic simulation of the impact of reinjected gas quantity on production, emissions, and overall irreversibilities across the oil value chain.

2. Methodology and tools

2.1. Exergy computation methodology

2.1.1. Stream exergy computation method

In the context of our study, the exergy of a fluid in any phase was calculated using a homogeneous thermodynamic approach [11]. The total specific molar exergy of the fluid is broken down into its physical molar exergy, related to differences in pressure and temperature, its chemical molar exergy, related to differences in composition with the environment, and its potential exergy. For potential exergy, we use a reference altitude of $z_a = 0$ at the ocean surface. The kinetic exergy term is neglected. The total specific exergy is calculated according to equation (1) below:

$$b = [h(T,P,z) - h(T_0,P_0,z)] - T_0[s(T,P,z) - s(T_0,P_0,z)] + \sum_k z_k\left[b_k^{0,*} + RT_0\ln(z_k\phi_k)\right] + gz_a \qquad (1)$$

Based on the chemical composition of this fluid, as well as its temperature and pressure, it is possible to describe the physical state of the fluid using a three-phase flash at specified pressure and temperature. Then, each of the stable phases is progressively brought to the reference state in equilibrium with the environment, under ambient conditions arbitrarily set to T_0=288.15 K and P_0=101325 Pa (atmospheric pressure). The vapor phase from the first flash is then subjected to a second flash at P, T_0, and the equilibrium phases from this second flash are themselves flashed again at P_0, T_0. The same thermodynamic pathway is applied to the oil and aqueous phases from the first flash. Finally, the chemical exergy is calculated using the standard chemical exergies for ideal gases introduced by Szargut in 1989 [12] for each reference chemical element in the environment, according to equation (2). This approach considers the decomposition of stable elements at reference concentrations in the environment into simple pure constituent substances q, followed by their recombination into the element of interest k.

$$b_k^{0,*} = \Delta_f G_k^0 + \sum_q \nu_q RT_0 \ln\left(\frac{P_0}{P_q}\right) \qquad (2)$$

Since most of the chemical elements making up the fluids modelled in this study are hydrocarbons, the stable reference elements in the environment considered for calculating chemical exergy are mainly carbon dioxide and water, at atmospheric concentrations updated according to the work of Rivero et al [13]. Finally, the various non-ideality terms related to the mixture are calculated in our approach directly using the residual quantities in the enthalpies and entropies at constant composition for physical exergy, and in the residual free enthalpy term, $z_k RT_0 ln(z_k\phi_k)$ for chemical exergy.

2.1.2. Exergy balance computation method

The model proposed in this study simulates the offshore field over several years, using monthly time steps and assuming steady-state conditions for each month. Material, energy, and exergy balances are therefore applied in steady-state mode to each element of the system as follows:

$$\sum_j \dot{W}_j + \sum_{sc} \dot{Q}_{sc}\left(1 - \frac{T_0}{T_{sc}}\right) + \dot{n}_i(b_{ie} - b_{is}) = \dot{I} \qquad (3)$$

In our case, the surface process equipment of the Girassol field does not include any technology for heat recovery at the condensers of the gas compression lines or at the exhaust of the turbines. Therefore, the exergy heat flows exchanged at the surface process can be considered as irreversibility, since they systematically represent a loss of exergy [14]. Consequently, equation (3) becomes:

$$\sum_j \dot{W}_j + \dot{n}_i(b_{ie} - b_{is}) = \dot{I} \quad (4)$$

This methodology for calculating exergy balances was implemented in C++ within the BEST software [15] developed by the Company which is briefly described in section 2.2.2.

2.2. Subsurface and surface coupling model and validation

2.2.1. Girassol oil and gas chain

The Girassol field can be broken down into four main structural elements, which are detailed below and on the Figure 1:

- The vessel equipped with surface process installations, known as the FPSO (Floating Production Storage and Offloading), which contains the oil separation trains (high, medium, and low pressure), the gas recompression trains, as well as water reinjection pumps and rotating machinery.
- The gathering network, composed of 16 parallel pipelines (risers), each connected to a group of wells and a gas-lift injection system.
- The production wells, which are distributed across the three different reservoirs of the field.
- The three reservoirs of the field, the most significant of which gives its name to the FPSO, listed in order of production importance as Girassol, Rosa, and Jasmin.

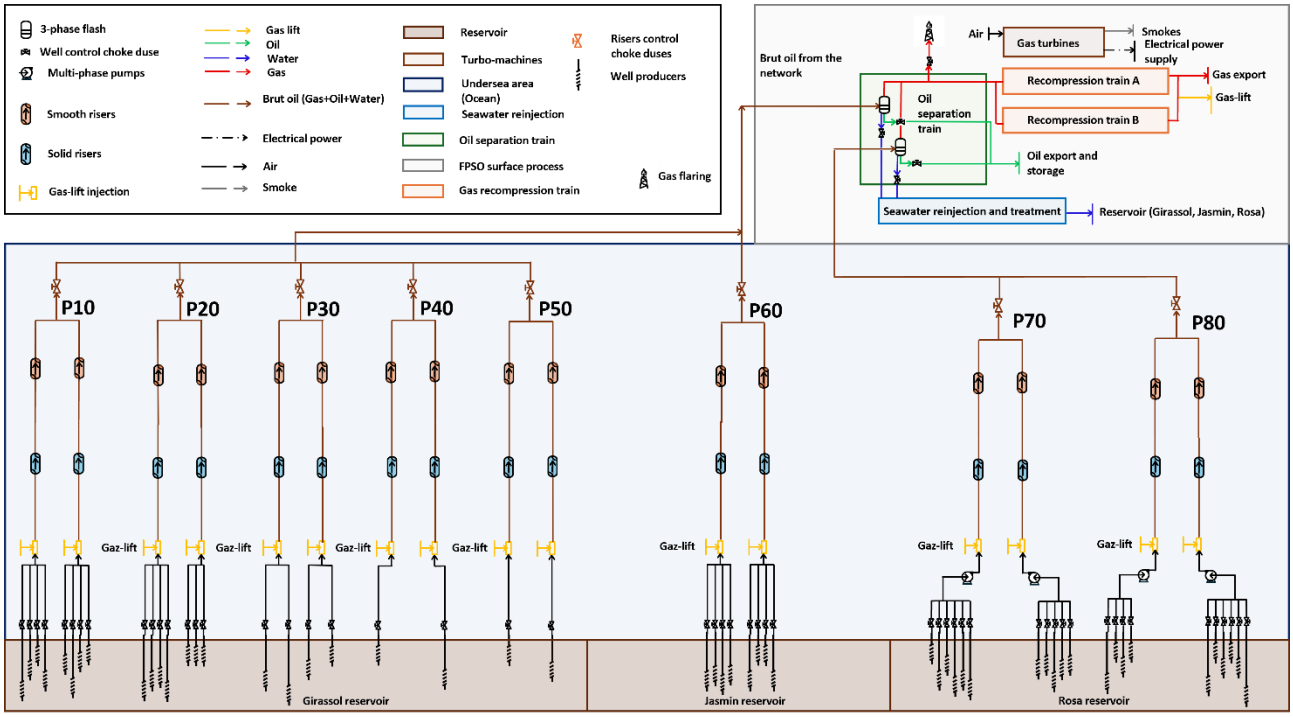

Figure. 1. *Girassol field flowsheet.*

2.2.2. Surface model

The BEST software is able to simulate steady state of surface process flowsheets including pumps, turbines, compressors, 2-phase or 3-phase flashes and so on. It also contains many thermodynamic models to compute enthalpy and entropy of streams needed in these modules and to perform phase equilibrium calculations. In our study we select the Peng-Robinson equation of state (1978) with the Soreid & Whitson modification (1992) to account for hydrocarbon-water interactions. Surface flowsheet, presented in Figure 2, is composed of different flashes allowing to separate gas, oil and aqueous if applicable phases and many gas turbines, pumps and compressors. Power production from two gas turbines (called turbogenerators 1 and 2 in Figure 2) is necessary to supply in electricity and mechanical work the electrical gas compressors from the LP and MP stages, recycling oil and water pumps, cooling loop and raw seawater pumps. Six turbo-compressors are used for the HP compression train A and B supplied by two turbines drivers called Turbo-compressors 1 and 2 in Figure 2. The last equipment consists of the two water reinjection pumps, each powered by its own driver turbine (called Turbo-pump 1 and turbo-pump 2 in Figure 2).

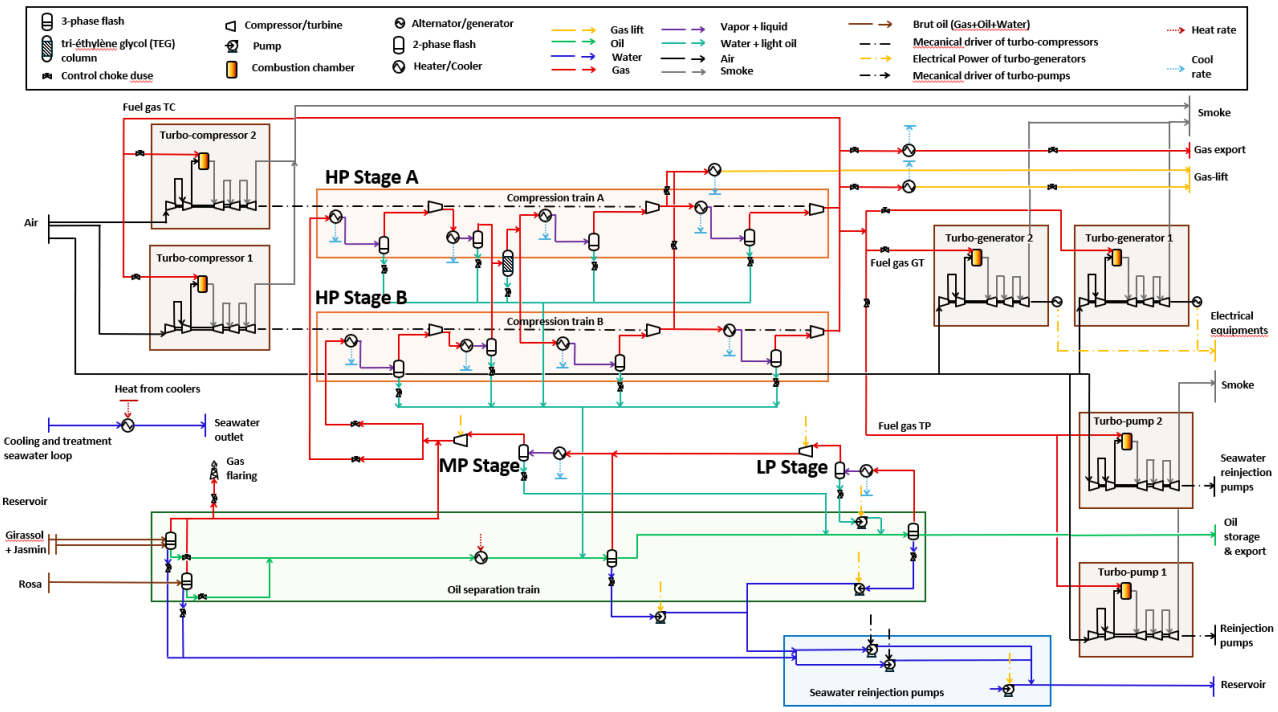

***Figure. 2**. Surface process flowsheet model in BEST software.*

All equipment except the gas turbines have been simulated using BEST. To correctly simulate the realistic operating point of the gas turbines on the Girassol FPSO, especially with a model that considers the real inlet parameters such as the ambient air temperature T_{air} and the power called $\dot{W}_{GT}$ at each turbine, a Python model, connected to BEST, has been designed to perform multiple bilinear interpolations and linear regressions on the available supplier curves datasets. Each data curve enables us to compute the fuel gas consumption flow rate and temperature of the exhaust gas produced as a function of the ambient air temperature in the compressor and the power called at the turbine. Moreover, as the turbine is usually commissioned within a specific callable power range, the interpolation on the supplier curves also enables us to determine the real available maximum power generated at the turbine depending on the ambient air temperature. Once all these data are computed a series of BEST (P, T) flash has been used to simulate respectively the air compressor state, the fuel gas entering in the combustor state and the exhaust gas state. The combustion reaction molar ratio has been considered stoichiometric. Then a molar, energetic and exergetic balances were performed at the boundaries of the gas turbine with the BEST flashes. Finally, to properly integrate these models in the optimization problem it was essential to include the shut-down state of the turbines, corresponding to zero consumed fuel gas flowrate, as well as zero exhaust flowrate, and a called power approaching zero. To achieve this, Bezier curves were calibrated between zero and the lower bounds of the supplier curves, characterized by an imposed slope, to ensure continuity and differentiability of the final extrapolated function. The results of this method are shown on the Figure 3, allowing the optimizer to correctly converge toward the shutdown state for switched off turbine. The results of the Figure 4 on the exergetic yield $\eta_{ex} = \dot{W}/\dot{B}_{fuel}$ estimated by the model are close but lower than the others exergy efficiency around 33 % found in the scientific literature [16]. This can be explained by the low energy efficiency of the gas turbine indicated in their supplier curves which are around 28 %. As mentioned in previous work [17] on gas turbine exergy modelling, the chemical exergy of the fuel gas is always slightly above the design heat consumption as the exergy computation thermodynamical transformation imply reversible path toward the environment conditions. Thus, in our case, the exergy efficiency of the gas turbine is lower than 28% precisely around 27 %. Then the gas turbine model results are consistent with the scientific literature explanation.

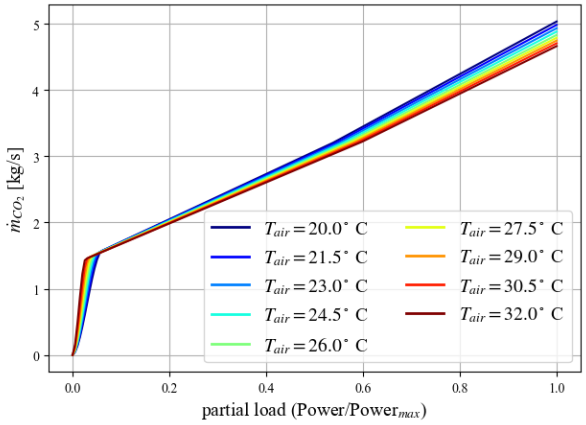

Figure 3. *CO_2 mass flowrate gas turbine model evolution depending on the load l=$\dot{W}/\dot{W}_{max}$*

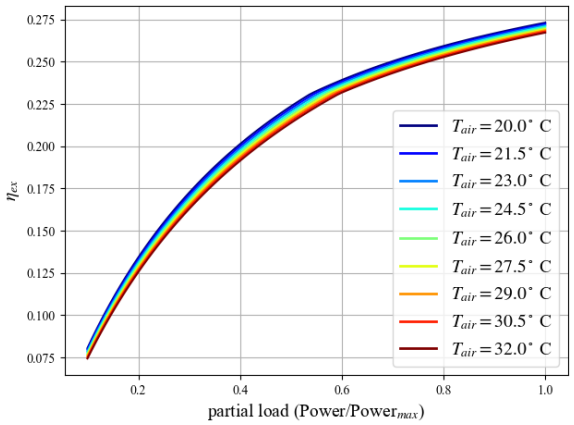

Figure 4 *Exergetic yield gas turbine model evolution depending on air temperature and the load.*

To precondition the upcoming optimization problem for distributing load rates between the turbines, the response surfaces shown on the Figure 5 and 6 for CO_2 emissions and model irreversibilities were post-processed as functions of the respective load rates of the two gas turbines across several ambient air temperatures. The model results indicate that for a given inlet air temperature, the response surfaces for CO_2 emissions and irreversibilities are very similar. This expected result allows us to hypothesize that the solution to the dynamic optimization problem for load sharing will be similar whatever the objective function to be minimized.

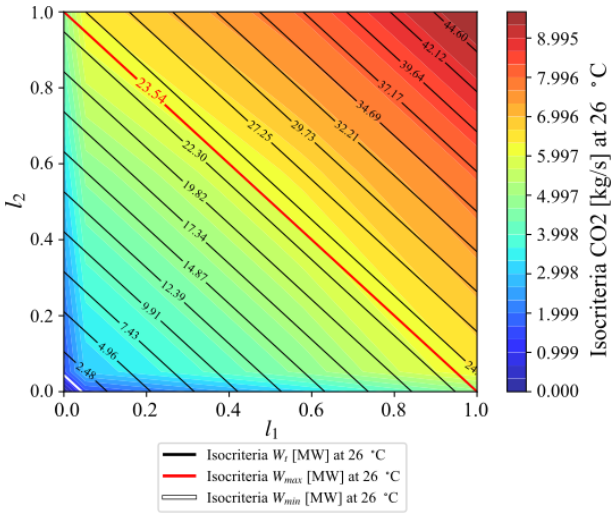

Figure 5 *CO_2 emissions domain model prediction at 26 (°C) air temperature.*

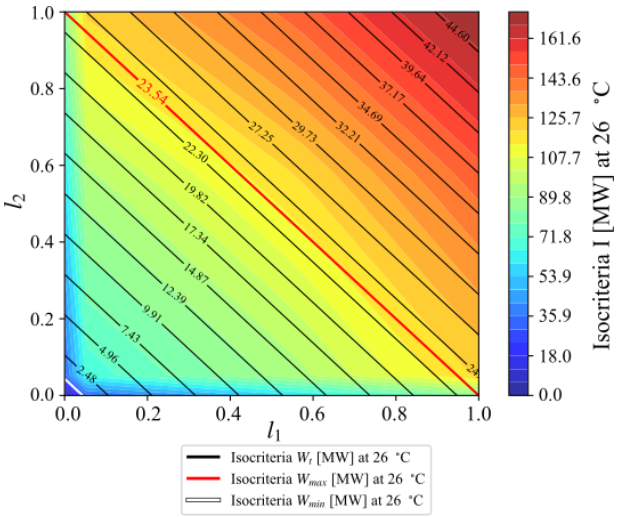

Figure 6 *Irreversibilities domain model prediction at 26 (°C) air temperature.*

2.2.3. Subsurface model

The modeling of the complete FPSO is based on a quasi-steady state approach. Both the subsurface and surface processes are calculated in steady state. But the conditions of the well are recalculated from step to step. The modeling of the subsurface equipment flowsheet has been done with the software GAP from the IPM Petroleum Engineer Expert PETEX software solution [18]. This tool is used by the Company to simulate the properties and the amount of each phase flowrate from the bottom of the wells to the top of the network thanks to the Black-Oil (BO) method. Girassol field is composed of three main reservoirs but in the BO model each well corresponds to a dataset of local reservoir conditions. We detail below this method just for one well at a time step t. First GAP applies linear interpolation using the well and reservoir dataset to determine, in function of the cumulated oil production $C_{oil}(t)$ the reservoir pressure Pres and the well bottom conditions: the well's productivity index IP (which depends on the geometry parameters of the completion and the mechanical properties of the fluid), the oil/gas ratio GOR, and the water/liquid ratio WCT. Then GAP computes the flowrate between the reservoir and the bottom of the well $\dot{V}_{lin}$ expressed as a function of IP and the difference between

the reservoir pressure P_{res} and the bottom hole pressure P_{bhp} : $\dot{V}_{lin} = IP(P_{res} - P_{bhp})$. Secondly GAP computes a dataset of the flowrate through the well, $\dot{V}_{lout}$, for various ranges of P_{whp} well head pressure. The correct liquid volumetric rate is deduced from the intersection between the $\dot{V}_{lin}$ and the corresponding $\dot{V}_{lout}$ curve shown on the Figure 7. The $\dot{V}_{oil}$ oil volumetric rate determined is added to the last cumulated oil production $C_{oil}(t)$ and then this new cumulated oil value, $C_{oil}(t + dt)$ is used to compute the new bottom well conditions. GAP releases this loop for each well. Once all the well's flowrates have been computed, GAP resolves the network mass and energy balances by using pressure loss correlations. Pipe's temperatures are computed independently by a thermal equation with no spatial dependency and a constant heat loss transfer coefficient depending on the pipe material and the surrounding temperature of the wall. This temperature is determined from an Angola sea water temperature dataset as a function of depth.

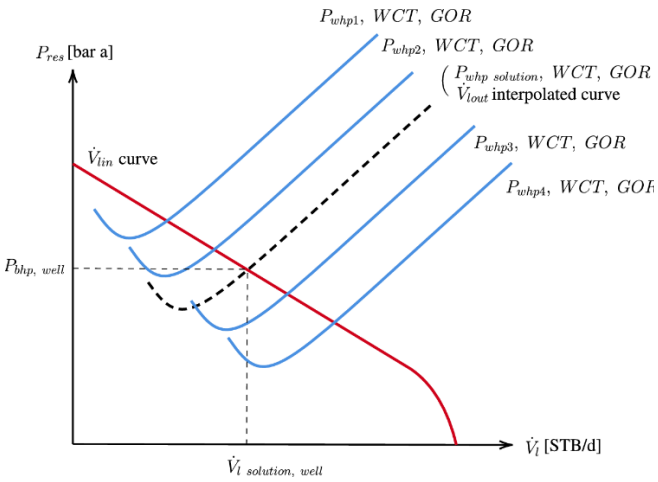

Figure 7 *$\dot{V}_{lin}$/$\dot{V}_{lout}$ intersection interpolation method*

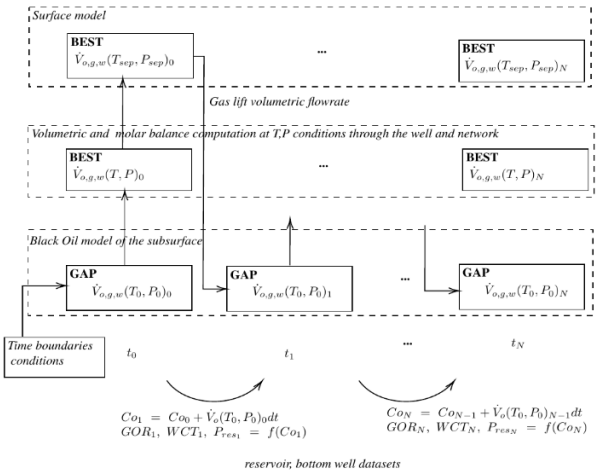

Figure 8 *Coupling workflow method GAP/BEST*

2.2.4. Coupling model and validation

The coupling between the two software packages involves on the one hand utilizing the BEST software, which enables exergy calculations and surface process simulation and on the other hand using GAP for the subsurface with the PETEX 'Open Server' API [18]. First the reservoirs are initialized with the corresponding historical cumulative production data as shown on the Figure 8, as well as gas lift density and molar composition. Once initialization is complete, allocation of the gas-lift flow rates in the risers can be set, subject to the surface maximum gas lift flow rate constraint. The GAP solver is then called to resolve the entire subsurface model and determine pressures, temperatures, and standard volumetric flow rates of oil, gas, and water at each node of the subsurface network, from the reservoirs to the inlet of the first surface three-phase separator as explain in the section 2.2.3. The BEST software then performs a mirror simulation of the GAP subsurface model to calculate the molar compositions corresponding to the standard flow rates at each node thanks to a sequence of pressure and temperature flashes at the bottomhole, wellhead, and gas lift injection nodes in the network. Then BEST performs a material and energy balance for the surface model. Finally, the gas turbine models are called to cover the site's power balance. Ultimately, BEST executes an exergy balance for the entire petroleum production chain. At the end of these calculations, the density and composition of the gas produced at time t and ready to be reinjected at time $t + dt$ is supplied to GAP (BEST to GAP), which has already calculated the new cumulated oil production $C_{oil}(t + dt)$. The dynamic simulation integrates this sequential loop until the simulation has reached the overall time horizon. The volumetric balance of the integrated model shows on the Figure 9 a maximum relative error under 10 % on the oil and gas rate over the entire field lifespan. Thus, the accuracy of the model is sufficient for optimising the oil and gas production. However, the error on the water rate increase to 5 ~ 15 % with the time. This error is due to the lack of accuracy of the IP historical dataset used by the Black Oil model from GAP to interpolate the IP of each well at each time step. Fixing historical IP will be imperative to achieve better result on the water flowrate. Nevertheless, the impact of these discrepancies on the water rate is not a limiting point for the optimization problems that will follow in this study as we are concerned more about the oil accuracy production. As expected, the Figure 10 shows that over 80 % of the irreversibility's of the site are due to the gas turbine and indirectly to the surface process.

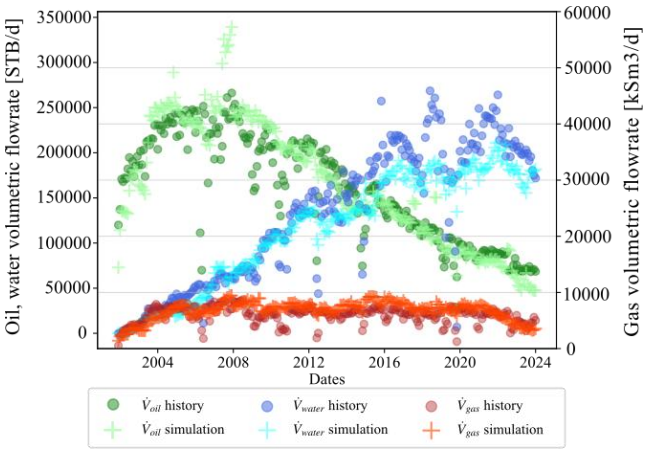

Figure. 9. *Oil, gas and water production history match*

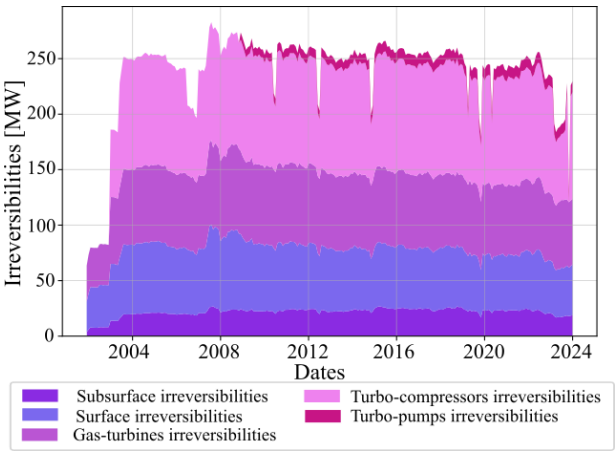

Figure. 10*. Irreversibilities simulation results*

3. Dynamic optimization studies

3.1. Gas turbines load allocation optimization problem

3.1.1. Gas turbines optimization model

The optimization of the turbogenerators involves determining the best way to distribute the electrical workload according to the real-time requirements of the surface processes. In fact, the surface process at the Girassol field includes three turbogenerators, which operate at partial load full-time, and one more serves as a backup in case a turbine fails, to supply power to the surface processes. The two turbines running at partial load generally provide between 25 and 30 MW of electrical power throughout the simulation time horizon. For this optimization problem, it is noteworthy that the choice of load distribution between the turbines depends only on variations in ambient air temperature at the gas turbine compressor inlets and the power demand to be supplied. Therefore, the objective function for this optimization problem is a black box based on the gas turbine model only and does not require simulating the entire coupled GAP+BEST model at each evaluation. To carry out this optimization, a simulation using the coupled model was performed once to obtain the profile of electrical power requirements for the equipment supplied by the turbogenerators. This power demand curve was then used as a time-dependent input parameter for the black box. Ultimately, the dynamic optimization problem is formulated as follows:

$$\underset{l_1(t),l_2(t)}{\text{Min}} \int_0^\tau C\dot{O}_2\big(l_i(t)\big)dt \quad or \quad \underset{l_1(t),l_2(t)}{\text{Min}} \int_0^\tau \dot{I}\big(l_i(t)\big)dt$$

$$\forall t \in [0,\tau] \quad l_1(t)\dot{W}_{max}(T_{air}(t)) + l_2(t)\dot{W}_{max}(T_{air}(t)) - \dot{W}_{GT}(t) = 0 \tag{5}$$

$$l_1(t) - l_2(t) > 0 \tag{6}$$

$$0 \le l_{1,2}(t) \le 1 \tag{7}$$

As explained previously, the modeling is performed discretizing the entire time horizon. The objective function is calculated using Simpson's method. The equality constraint (5) defines the coverage of the electrical demand required by the gas turbines. This equation includes the terms for the power demand assigned to each turbine, $l_i\,\dot{W}_{max}(T_{air}(t))$, where $l_i(t)$ is the turbine loading rate and $\dot{W}_{max}(T_{air}(t))$ is the maximum power available to the turbine at the ambient air temperature $T_{air}(t)$ at time t. Although it is considered that the evolution of the ambient air temperature at the gas turbines greatly affects their performance, the reference temperature for exergy calculation remains T_0. This assumption is strong, as physical exergy should ideally be referenced to the environment, but since the physical exergy term at the air inlet of the gas turbine is very small compared to the chemical exergy of the fuel gas, this assumption was maintained for the rest of the study. Inequality (6) expresses the symmetry of the problem, as seen in the gas turbine modeling results. Since the gas turbines are entirely similar in terms of their performance for the same input parameters, the optimization solution that calls turbine 1 at a loading rate of $l_1 = 1$ and the second at $l_2 = 0$ is completely equivalent to the opposite situation: $l_1 = 0$; $l_2 = 1$. Finally, the boundaries of the search domain are defined by inequality (7).

3.1.2. Gas turbine optimization results

The optimization strategy adopted for this problem involved using a deterministic SQP algorithm [19]. Since the search domain for the optimization problem is well-conditioned, with normalized load rate variables, a "LHS" or "Latin Hypercube Sampling" method was initially used to obtain a representative distribution of the search domain size. The SLSQP algorithm was then applied to all the initial x points obtained as shown on the Figure 11. Finally, filtering the best solutions allowed identification of the optimal curve on the Figure 12 for distributing the load rates between the turbines, according to whether CO_2 emissions or irreversibilities were selected as the objective function. These optimization results allow us to define the following rule below:

$$\forall t \in [0,\tau]\ l_i = \begin{cases} 0 \text{ or } 1 \text{ if } \dot{W}_{GT} \leq \dot{W}_{max}(T_0) \\ \frac{\dot{W}_{max}}{2\dot{W}_{GT}} \text{ if } \dot{W}_{GT} > \dot{W}_{max}(T_0) \end{cases} \quad (8)$$

This definition (8) of the gas turbine load value repartition has been implemented in the coupled model for future optimization problems. These results are confirmed in the literature regarding minimization of the entropy generation in complex systems [20],[21].

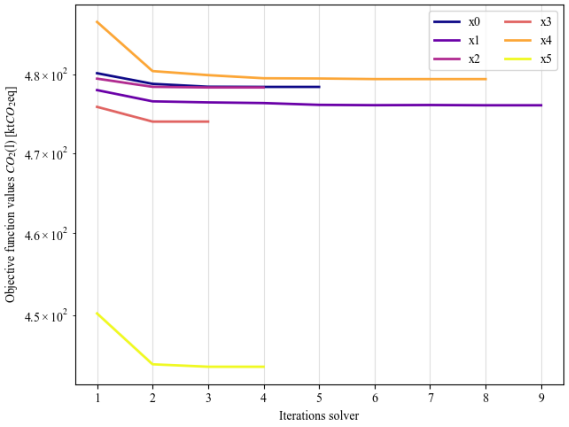

***Figure 11**. CO_2 emissions optimization solution convergence from LHS initial distribution.*

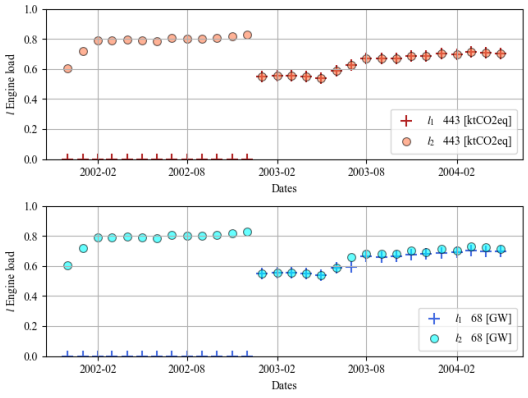

***Figure 12**. Best SLSQP dynamic optimization solution for both CO2 emissions and irreversibilities*

3.2. Gas lift allocation optimization problem

3.2.1. Gas-lift sensitivity

The current coupled model simulating the entire Girassol field with all gas-lift injections does not allow for the optimization of gas-lift flow distribution. The computational time required is far too high to attempt field-wide optimization, as there are 16 injection lines being simulated in parallel over roughly one-hundred-time steps, resulting in a very high-dimensional dynamic optimization model. Indeed 22 years of production with a monthly time step, thus 264-time steps correspond to 16×264=4224 degrees of freedom. Furthermore, a 22-year simulation takes several hours to compute, making the optimization problem too large to solve in its current form. However, attempting to resolve the issue as it stands is not optimal from a physical perspective, since not all gas-lift injections have the same impact on field production. It is thus necessary to first conduct a sensitivity analysis to identify the most important degrees of freedom regarding oil production.

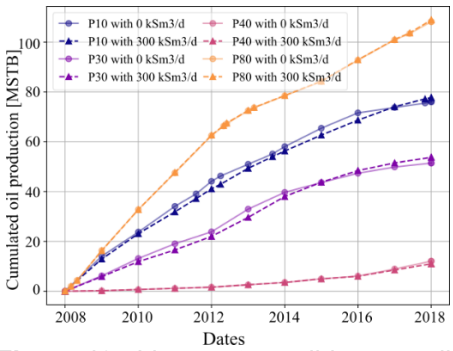

***Figure 13**. Lines not sensible to gas-lift*

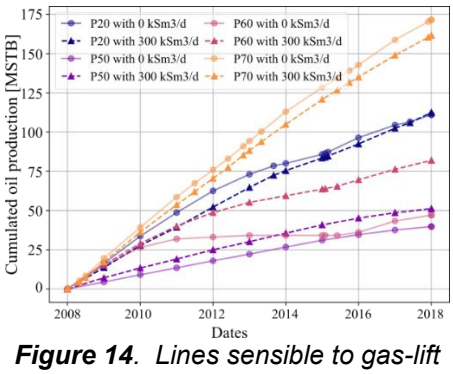

***Figure 14**. Lines sensible to gas-lift*

Accordingly, as shown on the Figure 13 and 14 a sensitivity analysis was first carried out on the different production lines of the Girassol field to identify the gas-lift injections mainly responsible for variations in oil production. The structure of the Girassol field, as previously described, includes several “risers” or production pipes within the gathering network between the wellheads and the first surface separator, into which the gas-lift flows are injected. This feature of Girassol’s architecture therefore allows for the separate optimization of each gas-lift injection line. In other words, each gas-lift flow directly affects only the production line (riser) into which it is injected and does not impact the other lines. As part of this sensitivity analysis, we suggest isolating the production lines with their gas-lift injection that contribute the most to the oil production variation. Then, it became possible to simulate the coupled model reproducing the historical production forecast without the line identified for optimization in the GAP and subsurface BEST models, using historical gas-lift flows for the other lines. This simulation yielded the different partial molar flows for all field lines except the line to optimize. Finally, a new model was built, allowing, this time, the GAP and subsurface BEST models to simulate only the production line to optimize, while ensuring that a surface feed source was added to the BEST model, incorporating the temporal evolution of partial molar flows from the first coupled simulation. This workflow is summarized in the Figure 15 below:

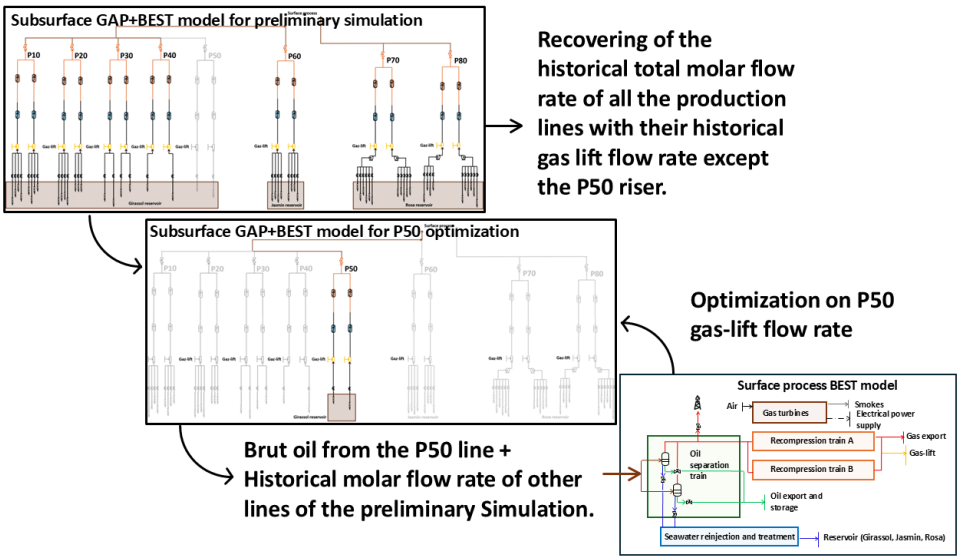

***Figure 15**. Workflow for the optimization of the P50 gas-lift line.*

Through this approach, a coupled GAP+BEST model was obtained, enabling only the simulation of the line to be optimized, while keeping historical production flows for all other lines. The time step size was also reduced to an annual time step size, with a shorter time horizon of 11 years. This resulted in a simulation computation time of 50 seconds with a problem size of 22 dimensions. Ultimately, according to the sensitivity analysis results, only three production lines are relevant for optimization from the gas-lift perspective: P20, P50, P60 and P70. In this study, we present optimization work on the P50 line, chosen for its simplicity, since it consists of only two producing wells.

3.3.2. Gas-lift optimization results

The model is a black box with an evaluation cost of 50 seconds, which simultaneously returns three different values for each evaluation: CO_2 emissions, irreversibilities, and cumulated oil production. Initially, the objective function considered was CO_2 emissions, with oil production as the constraint function. Subsequently, the objective function was changed to site irreversibilities, while maintaining oil production as the constraint. Regarding the optimization method implemented to solve this 22-dimensional problem, a first stochastic algorithm based on Bayesian inference by trust region [22], known as ‘TurBO’, was used to intelligently explore the search space to identify promising intermediate candidates. These candidates were then utilised as starting points by a deterministic solver of the SQP type, specifically the ‘SLSQP’ solver [19]. This method offers the considerable advantage of allowing parallelisation of the search, provided the black box model is process safe. Thus, the various points evaluated by the stochastic solver are initially assessed in parallel, followed by several deterministic calculations with SLSQP launched in parallel from these initial candidates. Another advantage of this combinatorial optimization method is that it enables comparison of the solutions achieved after

convergence of the different SLSQP runs, ensuring that the best solution found for each constraint is indeed a reliable optimum. The dynamic optimization problem is thus formulated as follows:

$$\begin{gathered}\underset{\dot{V}_{gl_i}(t)}{\text{Min}} \int_0^\tau C\dot{O}_2\left(\dot{V}_{gl_i}(t)\right)dt \quad ou \quad \underset{\dot{V}_{gl_i}(t)}{\text{Min}} \int_0^\tau \dot{I}\left(\dot{V}_{gl_i}(t)\right)dt \\ \forall t \in [0,\tau] \quad \dot{V}_{oil,c} - \epsilon \leq \sum_i \dot{V}_{oil_i} \leq \dot{V}_{oil,c} + \epsilon \\ \forall i \in N_l, \forall t \in [0,\tau]\ \dot{V}_{gl_i}(t) \in [0.0, 600.0]\ kSm3/day\end{gathered} \tag{9}$$

These two optimization problems were solved over a range of oil production constraint values, $\dot{V}_{oil,c}$. The constraint (9) is formulated as an inequality constraint within an ϵ-band around the reference value $\dot{V}_{oil,c}$. For example, with a $\dot{V}_{oil,c} = 820\,000\ kSTB$ we have admitted an ϵ error around $100\ kSTB$. The aim of generating an optimization Pareto curve allows us to compare the solutions based on the minimized objective function and to determine the potential gains between the historical gas lift flow distribution and the optimized one.

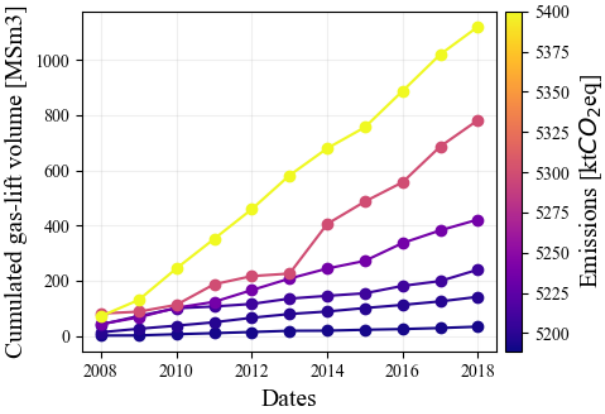

***Figure 16**. Dynamic optimization CO_2 gas lift solution*

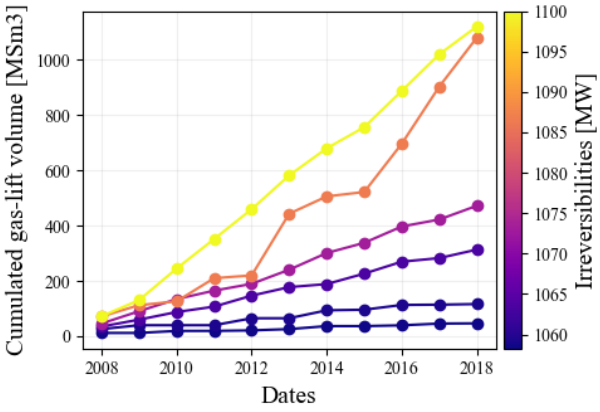

***Figure 17**. Dynamic optimization irreversibilities gas-lift solution*

In Figure 16 and 17, the results globally show that it is possible to produce the same amount of oil with a reduction of 30 % of the injected gas lift flow rate. In Figure 18, which shows the optimization Pareto curve, the black cross represents the CO_2 emissions simulated using the historical gas-lift rates. It can be observed that the final solution on the Pareto curve, which corresponds to an oil production constraint like the historical value, demonstrates that it is possible to meet the production constraint while reducing total emissions over 10 years by approximately 150 ktCO2eq, or about 3% of the historical emissions and around 30 MW of irreversibilities. In fact, the optimizer primary identified gas-lift injection rates much lower than the historical values. This confirms that the dynamic optimization of emissions appropriately accounts for whether it is more relevant to increase or decrease gas-lift injection depending on the time step. It is possible to achieve the same production level over the same time horizon by intelligently selecting the years when the wells should be activated by gas lift.

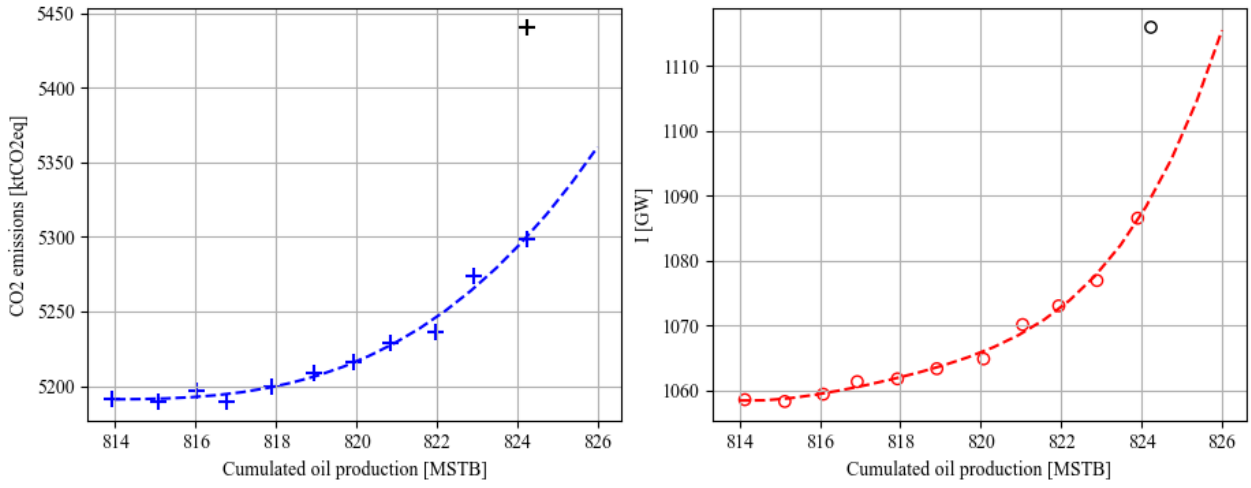

***Figure 18** : Dynamic optimization Pareto of both CO_2 emissions and irreversibilities*

4 Conclusions and perspectives

This dynamic optimization study applied to an integrated exergy model of an offshore oil and gas site which compares the carbon footprint and irreversibilities, has demonstrated three main points. First, **irreversibilities can easily be substituted for site CO_2 emissions as the objective function**, due to their strong dynamic correlation and, most importantly, their ability to minimize the carbon footprint while reflecting the site's energy performance. Secondly, results from the integrated exergy model show that **most of the site's irreversibilities are caused by the operation of gas turbines, specifically related to the management of gas recompression and gas-lift injection into the network, as well as other surface processes**. Finally, the optimization of the gas turbine load and gas-lift rate allocation significantly impact site performance. The optimal solution for the gas turbine loads allocation is the equal distribution and for gas-lift reducing the injection flow rate results in a **decrease of 3% of the CO_2 emissions at the same oil production constraint.** Future work will focus on two main topics. First find the optimal dynamic head pressure separation sequence. Despite the size of the model and its computational time cost with a proper method and formulation it would be possible on a short time horizon to see if the head pressure optimization can avoid CO_2 emissions and irreversibilities under oil constraints production. Secondly to try to optimize simultaneously the gas lift lines to capitalize the promising results of the P50 optimization.

Nomenclature

b	molar exergy, J/mol
C_{oil}	cumulated oil production, Sm^3
g	gravitational acceleration constant, m/s^2
h	molar enthalpy, J/mol
$\dot{I}$	irreversibilities, J/s
IP	well productivity index, $Sm^3/(s\times Pa)$
l	load of the gas turbine,
N_l	number of production line,
$\dot{n}$	molar flowrate, mol
P	pressure, Pa
P_{bhp}	bottom hole pressure, Pa
P_{res}	reservoir pressure, Pa
P_{whp}	well head pressure, Pa
P_q	partial pressure for the q element, Pa
$\dot{Q}$	heat exchange, J/s
R	Ideal gas constant, J/(mol×K)
s	molar entropy, J/(mol×K)
T	temperature, K
T_{sc}	heat source temperature, K
t	time, s
$\dot{V}_{gl}$	gas-lift volumetric injection rate, m^3/s
$\dot{V}_{lin}$	inlet volumetric liquid rate, m^3/s
$\dot{V}_{lout}$	outlet volumetric liquid rate, m^3/s
$\dot{V}_{oil}$	oil volumetric rate, m^3/s
$\dot{V}_{oil,c}$	oil volumetric rate constraint, m^3/s
$\dot{W}$	work exchange, J/s
z	molar composition,
z_a	depth, m
$\Delta_f G^0$	Gibbs free enthalpy of formation, J/mol

Greek symbols

ϵ	error on oil constraint
ϕ	fugacity coefficient
ν	stoichiometric reaction coefficient

Index

i stream or gas-lift line index.

ie inlet stream index

is outlet stream index

j shaft work source index

sc heat source index

k chemical component index

q pure simple chemical component index

References

[1] TotalEnergies, Sustainability and Climate Progress Report; 2025.

[2] E.Sciubba, G.Wall, A brief Commented History of Exergy From the beginnings to 2004, Journal of Thermodynamics; 2007; 10-1: 1-26.

[3] T.V.Nguyen, T.Jacyno, P.Breuhaus, M.Voldsund, B.Elmegaard, Thermodynamic analysis of an ups tream petroleum plant operated on a mature field., Energy; 2014;68: 464-469.

[4] J.A.M.da Silva, S. de Oliveira Jr, Unit exergy cost and CO2 emissions of offshore petroleum produc tion, Energy; 2018; 147: 757-766.

[5] T.V.Nguyen, L.Pierobon, B.Elmegaard, F.Haglind, P.Breuhaus, M.Voldsund, Exergetic assessment of energy systems on North Sea oil and gas platforms, Energy; 2013; 62: 23-36.

[6] M.Voldsund, T.V.Nguyen, B.Elmegaard, I.S.Ertesv˚ ag, A.Røsjorde, K.Jøssang, S.Kjelstrup, Exergy destruction and losses on four North Sea offshore platforms: A comparative study of the oil and gas processing plants., Energy; 2014; 74: 45–58.

[7] T.V.Nguyen, M.Voldsund, B.Elmegaard, I.S.Ertesv˚ ag, S.Kjelstrup, On the definition of exergy eff- iciencies for petroleum systems: Application to offshore oil and gas processing, Energy; 2014; 73: 264- 281.

[8] M.Voldsund, T.V.Nguyen, B.Elmegaard, I.S.Ertesv˚ ag, S.Kjelstrup, Thermodynamic performance indicators for evaluation of North Sea oil and gas platforms, Journal of Oil and Gas facilities; 2014; 3: 51-63.

[9] S. de Oliveira Jr, M. Von Hombeeck, Exergy analysis of Petroleum separation processes in offshore platforms, Energy convers, Institute for Technological Research and Polytechnic School of the Uni versity of Sao Paulo; 1997; 38-15: 1577-1584.

[10] M.Akchiche, Analyse exergétique et optimisation dynamique des systèmes de production d'hydro carbures dans la perspective de réduire les émissions de CO2, Université de Pau et des pays de l'Adour, 2020.

[11] S.Gourmelon, Méthodologie d'analyse et de rétro-conception pour l'amélioration énergétique des procédés industriels, INP Toulouse, 2015.

[12] J.Szargut, Chemical exergy of the Elements, Applied energy;1989; 32: 269-286.

[13] R.Rivero, M.Garfias, Standard chemical exergy of elements updated, Energy;2006; 31.

[14] R.Benelmir, Analyse exergétique- Applications, Energies- Physique énergétique 2019.

[15] BEST Basic Element for Simulation in Thermodynamic, BEST TotalEnergies's software, v13.0, 2025.

[16] T.Morosuk, G.Tsatsaronis, Advanced Exergy Analysis for Chemically Reacting Systems – Application to a Simple Open Gas-Turbine System, Journal of Thermodynamics; 2009: 105-111.

[17] D.Favrat, M.Kane, From the fuel heating values to the fuel exergy value in advanced energy systems, ECOS 2023: Proceedings of the 36th International Conference on Efficiency, Cost, Optimization, Simulation, and Environmental Impact of Energy Systems, 2023.

[18] PETEX Petroleum Experts Limited, IPM GAP Multiphase Flow Production Optimiser, v14.0, 2022.

[19] Lawson, C.L., R.J.Hanson, Solving Least Squares Problems, SIAM, Philadelphia, PA, 1995.

[20] B.Kilkis, Is exergy destruction minimization the same thing as energy efficiency maximization? Journal of Energy Systems;2021: 165-184.

[21] A.Bejan, Entropy generation minimization: The new thermodynamics of finite-size devices and finite- time processes, Journal of Applied Physics;1995; 79.

[22] D.Eriksson, M.Pearce, J.Gardner, R.Turner, and M.Poloczek, Scalable Global Optimization via Local Bayesian Optimization, Advances in Neural Information Processing Systems; 2019; 5496-5507; http://papers.nips.cc/paper/8788-scalable-global-optimization-via-local-bayesian-optimization.pdf.